Elastic anisotropy and shear-induced atomistic deformation of tetragonal silicon carbon nitride

Haiyan Yan, Meiguang Zhang, Yaru Zhao, Qun Wei, and Xinchun Zhou

Citation: Journal of Applied Physics **116**, 023509 (2014); doi: 10.1063/1.4889931
View online: http://dx.doi.org/10.1063/1.4889931
View Table of Contents: http://scitation.aip.org/content/aip/journal/jap/116/2?ver=pdfcov
Published by the AIP Publishing

Elastic anisotropy and shear-induced atomistic deformation of tetragonal silicon carbon nitride

Haiyan Yan,[1,a)] Meiguang Zhang,[2] Yaru Zhao,[2] Qun Wei,[3] and Xinchun Zhou[2]
[1]*College of Chemistry and Chemical Engineering, Baoji University of Arts and Sciences, Baoji 721013, People's Republic of China*
[2]*Department of Physics and Information Technology, Baoji University of Arts and Sciences, Baoji 721016, People's Republic of China*
[3]*School of Physics and Optoelectronic Engineering, Xidian University, Xi'an 710071, People's Republic of China*

(Received 31 May 2014; accepted 30 June 2014; published online 11 July 2014)

First-principles calculations are employed to provide a fundamental understanding of the structural features, elastic anisotropy, shear-induced atomistic deformation behaviors, and its electronic origin of the recently proposed superhard *t*-SiCN. According to the dependences of the elastic modulus on different crystal directions, the *t*-SiCN exhibits a well-pronounced elastic anisotropy which may impose certain limitations and restrictions on its applications. The further mechanical calculations demonstrated that *t*-SiCN shows lower elastic moduli and ideal shear strength than those of typical hard substances of TiN and TiC, suggesting that it cannot be intrinsically superhard as claimed in the recent works. We find that the failure modes of *t*-SiCN at the atomic level during shear deformation can be attributed to the breaking of C-C bonds through the bonding evolution and electronic localization analyses. © *2014 AIP Publishing LLC*.
[http://dx.doi.org/10.1063/1.4889931]

I. INTRODUCTION

A particular challenge in material sciences is the synthesis and design of materials with desired physical and chemical properties. It is for this reason that (super) hard materials have attracted significant interest.[1] The prediction of hexagonal β-C_3N_4[2,3] with extraordinary hardness has led to a great deal of experimental works synthesizing this novel CN material with different approaches.[4–10] However, the growth of β-C_3N_4 with crystal sizes large enough to enable measurement of its properties has not been achieved so far. In contrast to the β-C_3N_4, three different stable polymorphs of Si_3N_4 (α-, β-, and γ-Si_3N_4)[11–14] have been well-characterized with properties that make them useful for applications in which wear resistance is required at high temperatures and in a corrosive environment. Especially, the measured Vickers hardness of γ-Si_3N_4 is between 35 GPa[15] and 43 GPa[16,17] and confirms that this material qualifies as a potentially superhard solid. From the point of view of fabrication of ceramic composite materials, it has been suggested[18–20] that the incorporation of SiC into Si_3N_4 matrices can increase hardness, creep, and oxidation resistance properties compared to those in pure Si_3N_4 materials. Therefore, extensive experimental and theoretical efforts have turn to the synthesis and design of ternary Si-C-N ceramic materials with excellent chemical stability, high hardness, promising thermal properties, etc. Until recently, a great experimental achievement has led to the actual synthesis of Si-C-N materials and suggested possible applications using various techniques.[21–27] However, most these methods grow either rod-shaped crystal, mixtures of crystalline and amorphous, or pure amorphous $Si_{1-x-y}C_xN_y$ films for the tenability of atomic ratio in Si-C-N systems over a very wide range. Few uniform crystalline structures were obtained in Si-C-N materials, which are the key to understand the electronic and mechanical properties for actual applications.

In 1997, two crystalline solids, cubic SiC_2N_4 (space group, *Pn*3*m*) and orthorhombic Si_2CN_4 (space group, *Aba*2) in the ternary Si-C-N systems have been synthesized and determined by X-ray powder diffractions.[28] As demonstrated in the previous work,[29] the long chains of Si−N=C=N−Si fragments in these two structures limit their achievable hardness and the flexibility of the N=C=N bonds have been considered an essential feature for more extended structures. Following these pioneering works, extensive investigations have been carried out for predicting and designing other candidates for SiC_2N_4 and SiC_2N_4 with excellent mechanical properties.[29–36] Another promising cubic crystal phase, *c*-SiCN (space group, *F*–43 m), was experimentally determined and then made part of International Crystal Structure Database (ICSD).[37] More recently, Cui *et al.*[38] performed an extensive structural search of SiCN compounds, and a superhard tetragonal *t*-SiCN structure (space group, $P4_2nm$) was found to be the most preferential ground-state structure instead of *c*-SiCN. The formation energy calculations[38] have demonstrated that *t*-SiCN is thermodynamic stability[39,40] and could be experimentally synthesized at ambient pressures. As a novel SiCN single crystal phase, the theoretical hardness of *t*-SiCN is estimated to be 41.5 GPa by Cui *et al.* using the semi-empirical microscopic model of hardness. Nevertheless, it is a bit surprising that such a superhard material possesses a so low shear modulus of 174 GPa which is lower than the measured value of β-SiC (192 GPa).[41] In

[a)]Author to whom correspondence should be addressed. Electronic mail: hyyan1102@163.com

present work, we have extended the mechanical properties of *t*-SiCN and presented in detail the variations of the elastic moduli along the arbitrary directions. Moreover, in order to provide a deeper insight into mechanical behavior and hardness of this new SiCN phase, the stress-strain relations and the underlying atomistic bond breaking processes under the applied strain of *t*-SiCN were thus systematically studied.

II. THEORETICAL METHOD AND COMPUTATIONAL DETAILS

All first-principles plane wave calculations within density functional theory were performed using the Vienna *Ab-initio* Simulation Package (VASP).[42] The electronic exchange-correlation potential was treated by the generalized gradient approximation with the Perdew-Burke-Ernzerhof flavor.[43] The electron and core interactions were included by using the frozen-core all-electron projector augmented wave (PAW) method,[44] with Si: $3s^2 3p^2$, C:$2s^2 2p^2$, and N: $2s^2 2p^3$ treated as the valence electrons. Tests of the computational parameters showed that converged results (1 eV/atom) of the Kohn-Sham equations can be obtained with a plane-wave energy cutoff of 800 eV and a proper Monkhorst-Pack grid[45] ($10 \times 10 \times 6$) in the first Brillouin zone. The independent elastic constants were determined from evaluation of stress tensor generated small strain and bulk modulus, shear modulus, Young's modulus, and Poisson's ratio were thus estimated by the Voigt-Reuss-Hill approximation.[46] The stress-strain relationships were calculated by incrementally deforming the model cell in the direction of the applied strain, and simultaneously relaxing the cell basis vectors conjugated to the applied strain, as well as the positions of atoms inside the cell, at each step.[47,48] To ensure that the strain path is continuous, the starting position at each strain step has been taken from the relaxed coordinates of the previous strain step.

III. RESULTS AND DISCUSSIONS

Figure 1 shows the crystal structure of *t*-SiCN, in which the equivalent puckered SiCN hexagons are connected with each other by twisting alternately 90° so as to form three-dimensional intersecting honeycomb-stacks running along *c* axes. Further inspections reveal that the Si and C atoms are all tetrahedrally bonded and each N atom forms two Si-N bonds and one single C-N covalent bond. The equilibrium structural parameters for *t*-SiCN are calculated by full relaxations of both lattice geometry and ionic positions at ambient pressure. The optimized lattice constants of $a = 4.123$ Å and $c = 6.848$ Å, bond lengths of $d_{Si-C} = 1.914$ Å, $d_{Si-N} = 1.765$ Å, $d_{C-C} = 1.643$ Å, and $d_{C-N} = 1.465$ Å for *t*-SiCN are in good agreement with the recent theoretical values:[38] $a = 4.069$ Å, $c = 6.788$ Å, $d_{Si-C} = 1.889$ Å, $d_{Si-N} = 1.740$ Å, $d_{C-C} = 1.628$ Å, and $d_{C-N} = 1.458$ Å, differ only by 1.3%, 0.9%, 1.3%, 1.4%, 0.9%, and 0.5%, respectively. The agreement of our calculated structural parameters with the predicted results shows the accuracy and reliability of the present calculations.

We have plotted the band structure, total, and partial density of state (DOS) of *t*-SiCN at ambient pressure in Figure 2, where the horizontal dashed line is the Fermi level

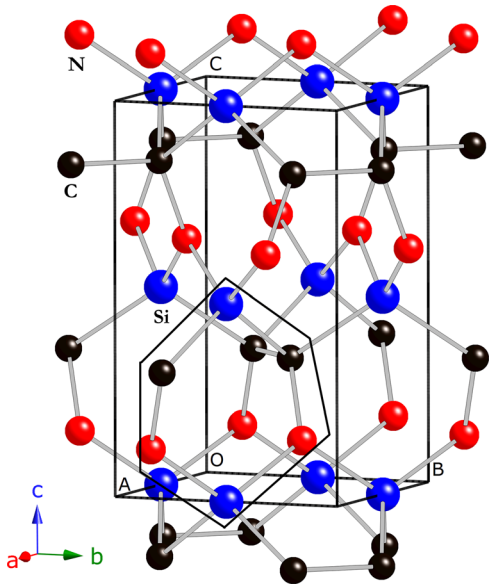

FIG. 1. Single crystal structure of *t*-SiCN, the blue, black, and red spheres represent Si, C, and N atoms, respectively.

(E_F). It can be seen that this tetragonal phase is an indirect band gap semiconductor with a band gap of 0.77 eV, which is close to the previous predicted value (0.89 eV).[38] From inspection of its partial DOS curves in Figure 2(c), it reveals that the valence band regions below E_F are mainly contributed by N-*p*, C-*p*, and Si-*p* states. Moreover, the N-*p* orbital has a significant hybridization with C-*p* and Si-*p* orbital localized in the energy range from −12 eV to E_F, indicating the strong C-N, Si-N, and Si-C covalent bonding nature in *t*-SiCN. We found through Bader charge analysis that the charge transfer from Si to N and C atom is 0.97 *e* and 1.83 *e* in one formula unit, indicating the ionicity of Si-C and Si-N bonds. Therefore, the chemical bonding in *t*-SiCN is a complex mixture of covalent and ionic characters.

The elastic stabilities, incompressibility, and rigidity of *t*-SiCN were determined from the calculated single crystal elastic constants by applying a set of given strains with a finite variation between −0.01 and +0.01. Table I listed the calculated elastic constants C_{ij} and derived Hill elastic moduli of *t*-SiCN along with the available theoretical values of *t*-SiCN[38] and experimental data[49,50] of TiN and TiC for comparisons. It can be seen that our calculated elastic constants C_{ij} and derived Hill elastic moduli are in reasonable agreement with those in Ref. 38. The calculated five independent elastic constants for *t*-SiCN satisfy the Born stability criteria,[51] thus suggesting that the tetragonal structure of *t*-SiCN is mechanically stable. In addition, the calculated results of *t*-SiCN showed that the elastic constants possess the trend $C_{11} < C_{33}$, indicating that *t*-SiCN is less compressible along the *c* axis than in the basal *a*-*b* plane. Moreover, it should be noted that the zero-pressure bulk modulus (B_0) derived from the third-order Birch-Murnaghan equation of state[52] agrees well with the derived Hill bulk modulus (B_H) in Table I, which demonstrates the good accuracy of our elastic calculations. However, it can be seen from Table I that the bulk and shear moduli of *t*-SiCN are, respectively, 37.7% (4.8%) and 17.3% (12.3%), lower than those of typical hard substances

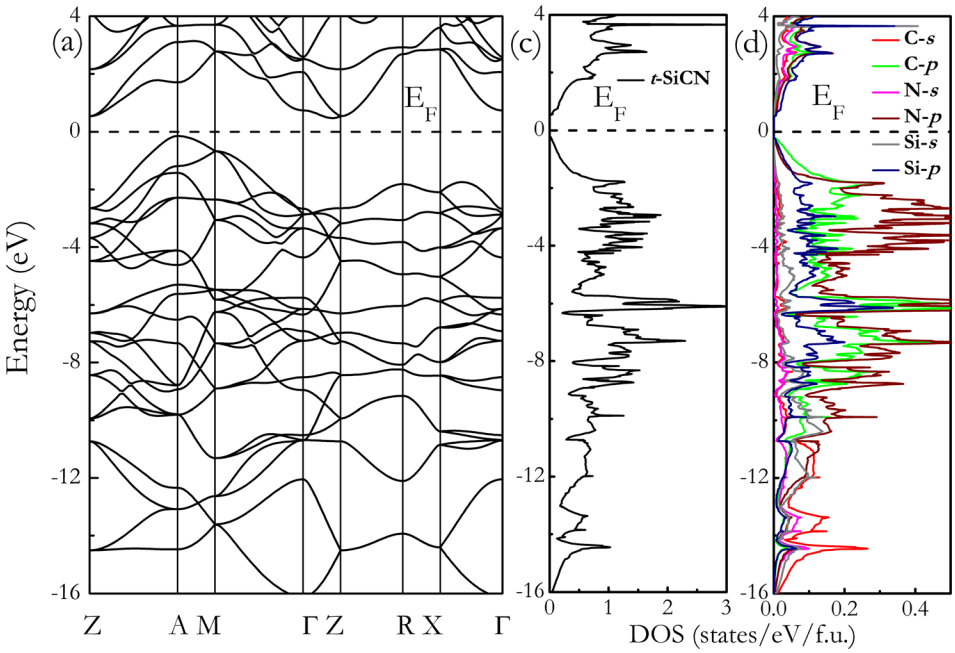

FIG. 2. Band structure (a), total (b), and partial DOS (c) of *t*-SiCN at ambient pressure.

of TiN (TiC),[49,50] indicating the lower rigidity and high compressibility for *t*-SiCN. Considering that the shear modulus can be a measure of the resistance to plastic deformation and the bulk modulus can be a measure of the resistance to fracture by an external force, the critical *G*/*B* ratio which separates ductile and brittle materials is around 0.57,[53] i.e., if $G/B < 0.57$ the material behaves in a ductile manner, otherwise the material behaves in a brittle manner. As shown in Table I, the calculated *G*/*B* ratio for *t*-SiCN is 0.7, suggesting its brittle behaviors. To understand the elastic anisotropy of *t*-SiCN on a fundamental level, we have calculated the orientation dependences of the Young's modulus *E* and shear modulus *G*, as shown in the Figure 3. The calculations of elastic moduli-crystal orientation dependences conducted here are similar to our previous studies to which we refer the reader for further details.[54] Figure 3(a) shows three-dimensional picture of dependence of the *E* on a direction in crystal, and the distance from the origin of system of coordinate to the closed surface equals to the *E* in a given direction. For a perfectly isotropic medium this three-dimensional surface should be a sphere, however, Figure 3(a) shows a well-pronounced anisotropy of *t*-SiCN. The cross-sections of *t*-SiCN in *ab* and *bc* plane are also shown in Figure 3(b), in which the calculated E_{max}/E_{min} ratio of the Young's moduli for *t*-SiCN is $E_{[001]}/E_{[100]} = 571/217 = 2.63$. In Figure 3(c), the orientation dependences of Young's modulus *E* along tensile axes within (001), (100), and $(1\bar{1}0)$ specific planes are plotted and the ordering of Young's modulus as a function of direction in *t*-SiCN is $E_{[001]} > E_{[111]} > E_{[011]} > E_{[110]} > E_{[100]}$. Similarly, the orientation dependences of the shear modulus *G* of the *t*-SiCN were also conducted for shear on (001), (100), and $(1\bar{1}0)$ planes, as plotted in Figure 3(d). It can be seen that the shear modulus of *t*-SiCN possesses its minimum value for shear on $(1\bar{1}0)[110]$ ($G_{(1\bar{1}0)[110]} = 71$ GPa) and its maximum value for shear on (100)[010] ($G_{(100)[010]} = 217$ GPa).

As mentioned above that the theoretical hardness of *t*-SiCN is estimated to be 41.5 GPa in Ref. 38, however, both the calculated bulk and shear moduli of *t*-SiCN in the present work are lower than those of the typical hard materials TiN and TiC. Previous publications[55–58] have demonstrated that ultimate hardness of a material may be assessed from its ideal shear strength, which also appears to correlate with the onset of dislocation formation in an ideal, defect-free crystal. The ideal strength in a specified direction is microscopically determined by bond strength and breaking nature under strain. The stress-strain relations upon tension and shear for the tetragonal *t*-SiCN are thus calculated and the obtained results are plotted in Figure 4. Figure 4(a) shows the stress-strain relations in different tension directions for *t*-SiCN. The ideal tension strengths, defined as the first maximum in the stress-strain curves, are 37.6 GPa, 79.7 GPa, 51.6 GPa,

TABLE I. Calculated single crystal elastic constants C_{ij} (GPa), Hill bulk modulus B_H (GPa) and shear modulus G_H (GPa), G_H/B_H ratio, and equation of state (EOS) fitted bulk modulus B_0 (GPa) for the *t*-SiCN.

Structure	Source	C_{11}	C_{33}	C_{44}	C_{66}	C_{12}	C_{13}	B_H	G_H	G_H/B_H	B_0
t-SiCN	Present	323.7	631.0	193.1	216.8	181.7	123.1	231	162	0.70	226
	Theory[38]	340.8	663.7	205.9	229.6	183.5	126.4	241	174[a]	0.72	
TiN	Exp.[49]	625		163		165		318	190		
TiC	Exp.[50]	500		175		113		242	182		

[a]Determined from the calculated elastic constants by the Voigt-Reuss-Hill approximation.

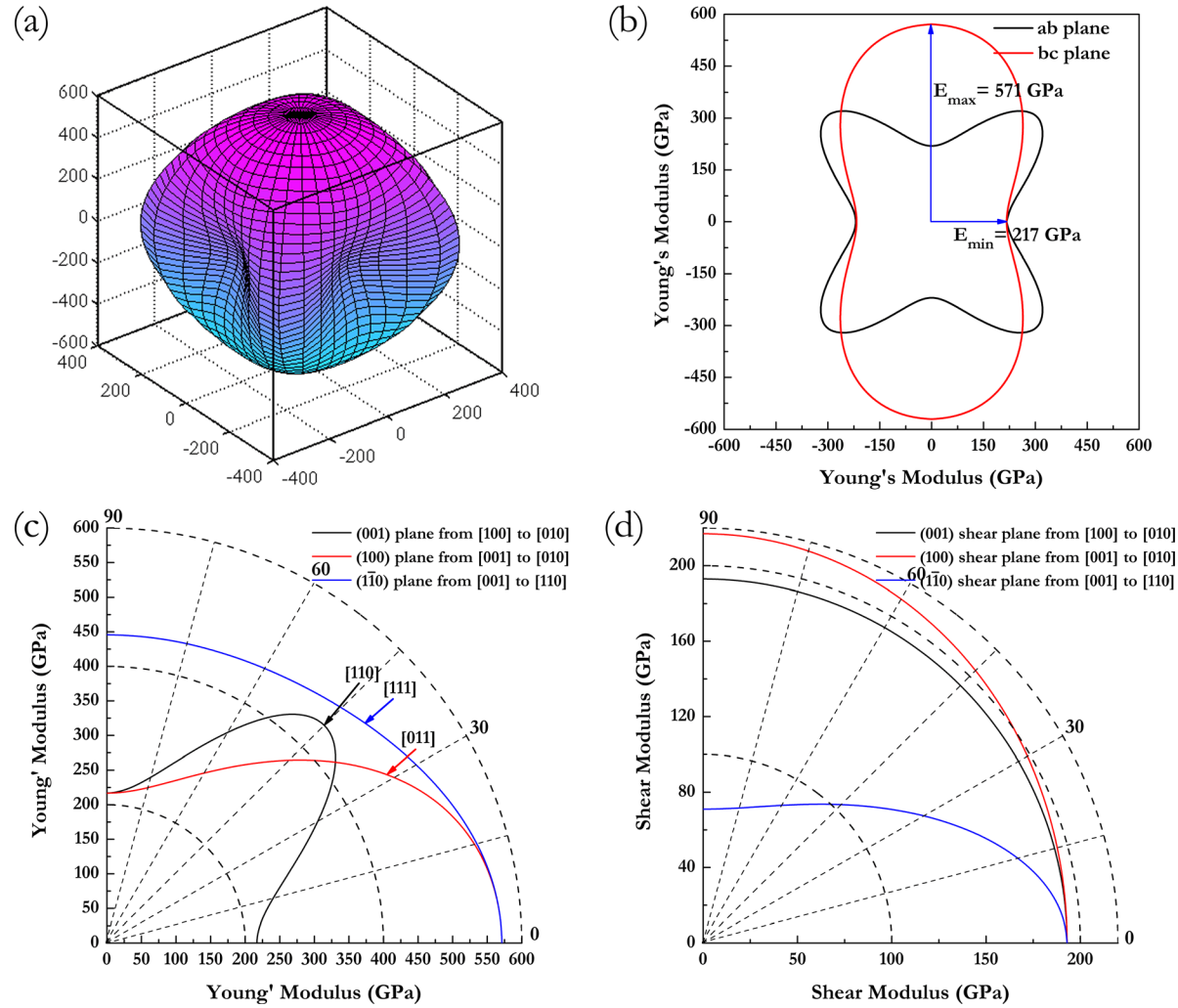

FIG. 3. Three-dimensional surface representations of the Young's Modulus E for t-SiCN (a), the corresponding projections in ab and bc plane for t-SiCN (b), orientation dependence of the Young's modulus (c), and orientation dependence of the shear modulus (d) in t-SiCN.

and 51.4 GPa along the ⟨100⟩, ⟨001⟩, ⟨110⟩, and ⟨111⟩ directions, respectively. The anisotropy ratio of ideal tensile strengths for t-SiCN is $\sigma_{\langle 100\rangle}$: $\sigma_{\langle 001\rangle}$: $\sigma_{\langle 110\rangle}$: $\sigma_{\langle 111\rangle} \approx 1$: 2.12: 1.37: 1.37. The lowest peak tensile stress for t-SiCN in the ⟨100⟩ direction is 37.6 GPa which is larger than the lowest tensile strengths of Re_2N ($\sigma_{\langle \bar{1}2\bar{1}0\rangle} = 28.5$ GPa) and Re_3N

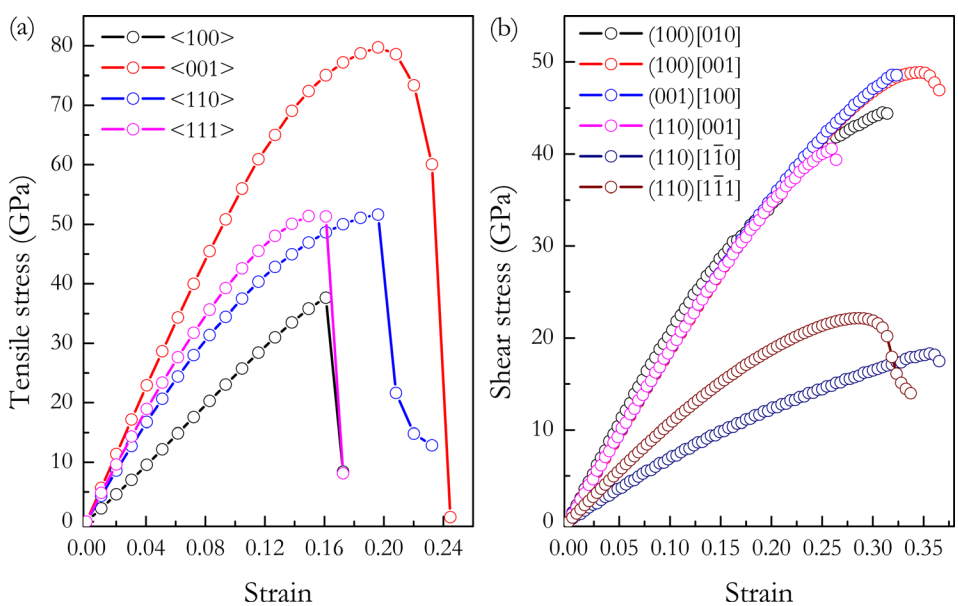

FIG. 4. Calculated stress-strain relations for t-SiCN in various tensile (a) and shear (b) directions.

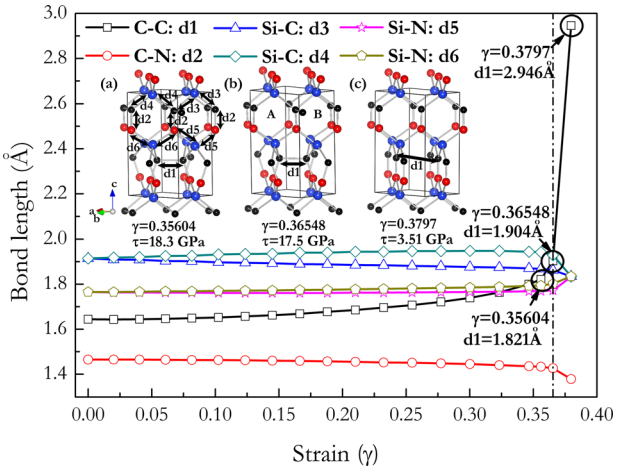

FIG. 5. Calculated bond lengths as a function of strain for *t*-SiCN under along (110) $[1\bar{1}0]$ shear directions. Insets: crystal structures before (a) and after (b) and (c) shear instability. The dashed line represents the shear-induced structural deformation firstly occurrence.

($\sigma_{\langle\bar{1}2\bar{1}0\rangle} = 34.5$ GPa),[57] but is lower than those of B_6O ($\sigma_{\langle10\bar{1}0\rangle} = 53.3$ GPa),[56] ReB_2 ($\sigma_{\langle\bar{1}2\bar{1}0\rangle} = 58.5$ GPa),[56] WB_3 ($\sigma_{\langle10\bar{1}0\rangle} = 43.3$ GPa),[58] γ-Si_3N_4 ($\sigma_{\langle110\rangle} = 41.2$ GPa),[59] and *c*-BN ($\sigma_{\langle111\rangle} = 55.3$ GPa).[60] The calculated stress-strain curves along principal shear paths in *t*-SiCN are shown in Figure 4(b), in which the highest shear strength of 48.9 GPa and the lowest shear strength of 18.3 GPa is found under the (100)[001] and (110) $[1\bar{1}0]$ shear loading, respectively. The lowest shear strength of *t*-SiCN (18.3 GPa) is much lower than the lowest shear strengths of B_6O ($\tau_{\langle0001\rangle\langle10\bar{1}0\rangle} = 38.0$ GPa),[56] WB_3 ($\tau_{\langle0001\rangle\langle10\bar{1}0\rangle} = 37.7$ GPa),[58] and *c*-BN ($\tau_{\langle111\rangle\langle11\bar{2}\rangle} = 58.3$ GPa).[60] In addition, this value is also lower than the lowest shear strengths of *fcc*-TiC (31.3 GPa) and *fcc*-TiN (29.1 GPa)[61] in the same (110) $[1\bar{1}0]$ slip system, respectively, showing its lower shear resistance or hardness than these materials. We thus estimated the hardness of *t*-SiCN using the Chen's model.[62] Indeed, the obtained hardness of *t*-SiCN is 22 GPa which is lower than the measured value of hardness of 28 GPa for TiC.[63] Therefore, both ideal shear strength and theoretical hardness indicate that *t*-SiCN is a common hard material, not a superhard material. In addition, it is found that the weakest shear strength of 18.3 GPa at a strain of 0.356 in the (110) $[1\bar{1}0]$ direction is lower than the weakest tensile strength of 37.6 GPa at a strain of 0.161 in the $\langle100\rangle$ direction. This means the failure mode in *t*-SiCN is dominated by the shear type in the (110) $[1\bar{1}0]$ direction.

To shed light on the origin of the intriguing bond-breaking pattern and atomistic deformation mechanism in (110) $[1\bar{1}0]$ direction, the variations of bond lengths and electronic structures as a function of applied strain were plotted in Figures 5 and 6, respectively. Under increasing shear strains, the equivalent puckered SiCN hexagons (see Figure 1) in *t*-SiCN at equilibrium state are evolved into two inequivalent SiCN hexagons denoted as A and B in the inset (b) in Figure 5. Correspondingly, the equivalent Si-C (Si-N) bond length in *t*-SiCN is splitted from one bond distance to two different bond distances indicated as *d*3 and *d*4 in B and A SiCN hexagons (*d*5 and *d*6 in B and A SiCN hexagons), respectively. More detaily, the C-N bonds denoted as *d*2 decreases slowly in the whole studied strain range, on the contrary, the C-C bonds denoted as *d*1 in *t*-SiCN are stretched increasingly and break at the critical shear strain of $\gamma = 0.36548$, which limits the achievable shear strengths of *t*-SiCN. Such a bond-breaking can also be clearly seen from the selected crystal structures before ($\gamma = 0.36504$) and after ($\gamma = 0.36548$ and $\gamma = 0.3797$) shear instability [see the insets (a), (b), (c) in Figure 5]. It means that this shear-induced structural deformation occurs at strain of $\gamma = 0.36548$ through the collapse of tetrahedron block including C-C bond in *t*-SiCN. Interestingly, the difference between *d*3 and *d*4 of Si-C bonds increases to 0.067 Å and the one between *d*5 and *d*6 of Si-N bonds increases to 0.03 Å at critical shear strain of $\gamma = 0.36548$ and then both of them decrease abruptly to zero along with the breaking of *d*1 bonds at shear strain of $\gamma = 0.3797$. Meanwhile, all of the Si-C and Si-N bond lengths are equal to 1.834 Å at this strain and this means that both A and B SiCN hexagons are equivalent again at shear strain of $\gamma = 0.3797$ by simultaneously breaking of C-C (*d*1) bonds. Therefore, the instability of C-C bonds under shear deformation for *t*-SiCN can be attributed to a local transformation of sp^3 to sp^2 bonding of C atoms upon the shear. In addition, the changes of the Electronic Localization Function (ELF) of *t*-SiCN upon shear deformation [(110) $[1\bar{1}0]$ direction] were analyzed to rationalize the deformation of C-C bonds. At ELF = 0.75, Figure 6 presents the electron localization distributions of *t*-SiCN at different strains of about 0.1664, 0.34665, 0.36504, 0.36548, and 0.3797, i.e., before and after the instability for the (110) $[1\bar{1}0]$ slip system. One can see that the ELF are similar at

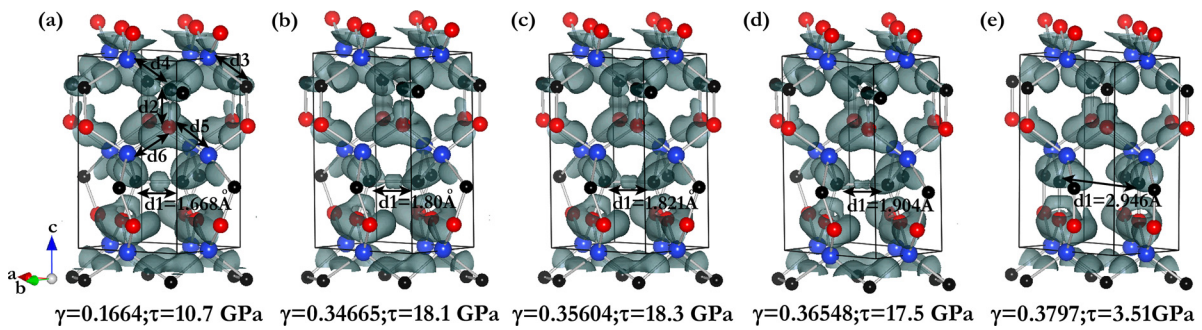

FIG. 6. Developments of ELF for *t*-SiCN during shear in the (110) $[1\bar{1}0]$ slip at different strains of 0.1664 (a), 0.34665 (b), 0.36504 (c), 0.36548 (d), and 0.3797 (e).

strains of 0.34665 and 0.36504 (before the shear instability), but a significant difference appears between C-C bonds at large strains of 0.36548 and 0.3797 (after the shear instability). Especially for ELF at strain of 0.3797 presented in Figure 6(e), where no electron localized at C-C bond and results in the breaking of this bond. Therefore, these ideal strength results indicate that this predicted *t*-SiCN is unlikely to become superhard material as previous theoretical suggested. Further experimental and theoretical works for *t*-SiCN are thus greatly encouraging.

IV. CONCLUSIONS

In summary, we have performed systematic first-principles calculations to examine the structural stability, Vickers hardness, tensile and shear strengths of *t*-SiCN which was claimed to be superhard. The resulting equilibrium properties are consistent with previous theoretical results. The calculations reveal the bulk and shear moduli of *t*-SiCN are 231 and 162 GPa, respectively, which are much lower than those of typical hard substances of TiN and TiC. The orientation dependence of the Young's modulus reveals that the *t*-SiCN is the stiffest along [001] and the most compliant along [100] in response to tensions. The substantially low shear strength and theoretical hardness of *t*-SiCN indicate that it is a common hard material. Detailed analyses of the failure modes for *t*-SiCN under shear deformation reveal that the breaking of C-C bonds is responsible for the lattice instability. The present calculations provide fundamental information for better understanding of structural stability and mechanical performance of this interesting material.

ACKNOWLEDGMENTS

This work was supported by the National Natural Science Foundation of China (Grant No. 11204007), the Natural Science Basic Research plan in Shaanxi Province of China (Grant Nos. 2012JQ1005, and 2013JQ1007), and Education Committee Natural Science Foundation in Shaanxi Province of China (Grant No. 2013JK0638).

[1]Y. J. Tian, B. Xu, and Z. S. Zhao, Int. J. Refract. Met. Hard Mater. **33**, 93 (2012).
[2]A. Y. Liu and M. L. Cohen, Science **245**, 841 (1989).
[3]A. Y. Liu and M. L. Cohen, Phys. Rev. B **41**, 10727 (1990).
[4]M. R. Wixom, J. Am. Ceram. Soc. **73**, 1973 (1990).
[5]C. Niu, Y. Z. Lu, and C. M. Lieber, Science **261**, 334 (1993).
[6]D. Marton, K. J. Boyd, A. H. Al-Bayati, S. S. Todorov, and J. W. Rabalais, Phys. Rev. Lett. **73**, 118 (1994).
[7]H. Sjöström, S. Stafström, M. Boman, and J.-E. Sundgren, Phys. Rev. Lett. **75**, 1336 (1995).
[8]H. Montigaud, B. Tanguy, G. Demazeau, I. Alves, and S. Courjault, J. Mater. Sci. **35**, 2547 (2000).
[9]C. B. Cao, Q. Lv, and H. S. Zhu, Diamond Relat. Mater. **12**, 1070 (2003).
[10]J. N. Hart, F. Claeyssens, N. L. Allan, and P. W. May, Phys. Rev. B **80**, 174111 (2009).
[11]G. Dufour, F. Rochet, H. Roulet, and F. Sirotti, Surf. Sci. **304**, 33 (1994).
[12]A. Zerr, G. Miehe, G. Serghiou, M. Schwarz, E. Kroke, R. Riedel, H. Fuess, P. Kroll, and R. Boehler, Nature **400**, 340 (1999).
[13]S. D. Mo, L. Ouyang, W. Y. Ching, I. Tanaka, Y. Koyama, and R. Riedel, Phys. Rev. Lett. **83**, 5046 (1999).
[14]B. Kiefer, S. R. Shieh, T. S. Duffy, and T. Sekine, Phys. Rev. B **72**, 014102 (2005).
[15]J. Z. Jiang, F. Kragh, D. J. Frost, K. Ståhl, and H. Lindelov, J. Phys.: Condens. Matter **13**, L515 (2001).
[16]I. Tanaka, F. Oba, T. Sekine, E. Ito, A. Kubo, K. Tatsumi, H. Adachi, and T. Yamamoto, J. Mater. Res. **17**, 731 (2002).
[17]A. Zerr, M. Kempf, M. Schwarz, E. Kroke, M. Goken, and R. Riedel, J. Am. Ceram. Soc. **85**, 86 (2002).
[18]P. Greil, G. Petzow, and H. Tanaka, Ceram. Int. **13**, 19 (1987).
[19]R. Raj and R. K. Borchia, Acta Metall. **32**, 1003 (1984).
[20]R. Riedel, M. Seher, and G. Becker, J. Eur. Ceram. Soc. **5**, 113 (1989).
[21]M. I. Baraton, W. Chang, and B. H. Kear, J. Phys. Chem. **100**, 16647 (1996).
[22]P. Jedrzejowski, J. Cizek, A. Amassian, J. E. Klemberg-Sapieha, J. Vlcek, and L. Martinu, Thin Solid Films **447–448**, 201 (2004).
[23]C. W. Chen, C. C. Huang, Y. Y. Lin, W. F. Su, L. C. Chen, and K. H. Chen, Appl. Phys. Lett. **88**, 073515 (2006).
[24]B. P. Swain and N. M. Hwang, Appl. Surf. Sci. **254**, 5319 (2008).
[25]D. Su, Y. L. Li, Y. Feng, and J. Jin, J. Am. Ceram. Soc. **92**, 2962 (2009).
[26]Y. Awad, M. A. ElKhakani, M. Scarlete, C. Aktik, R. Smirani, N. Camiŕ, M. Lessard, and J. Mouine, J. Appl. Phys. **107**, 033517 (2010).
[27]C. Guthy, R. M. Das, B. Drobot, and S. Evoy, J. Appl. Phys. **108**, 014306 (2010).
[28]R. Riedel, A. Greiner, G. Miehe, W. Dressler, H. Fuess, J. Bill, and F. Aldinger, Angew. Chem., Int. Ed. **36**, 603 (1997).
[29]H. B. Wang, Q. Li, H. Wang, H. Y. Liu, T. Cui, and Y. M. Ma, J. Phys. Chem. C **114**, 8609 (2010).
[30]C. Z. Wang, E. G. Wang, and Q. Dai, J. Appl. Phys. **83**, 1975 (1998).
[31]P. Kroll, R. Riedel, and R. Hoffmann, Phys. Rev. B **60**, 3126 (1999).
[32]J. E. Lowther, Phys. Rev. B **60**, 11943 (1999).
[33]J. E. Lowther, M. Amkreutz, T. Frauenheim, E. Kroke, and R. Riedel, Phys. Rev. B **68**, 033201 (2003).
[34]E. Betranhandy, L. Capou, S. F. Matar, and C. El-Kfoury, Solid State Sci. **6**, 315 (2004).
[35]X. Zhang, Z. Chen, H. Du, C. Yang, M. Ma, J. He, Y. Tian, and R. Liu, J. Appl. Phys. **103**, 083533 (2008).
[36]H. J. Du, L. C. Guo, D. C. Li, D. L. Yu, and J. L. He, Chin. Phys. Lett. **26**, 016403 (2009).
[37]Inorganic Crystal Structure Database (ICSD), FIZ Karlsruhe, # 28391, 2006/04/01.
[38]L. Cui, Q. Q. Wang, B. Xu, D. L. Yu, Z. Y. Liu, Y. J. Tian, and J. L. He, J. Phys. Chem. C **117**, 21943 (2013).
[39]C. Jiang, Z. J. Lin, and Y. S. Zhao, Phys. Rev. Lett. **103**, 185501 (2009).
[40]C. Jiang, Z. J. Lin, and Y. S. Zhao, Phys. Rev. B **80**, 184101 (2009).
[41]R. D. Carnahan, J. Am. Ceram Soc. **51**, 223 (1968).
[42]G. Kresse and J. Furthmüller, Phys. Rev. B **54**, 11169 (1996).
[43]J. P. Perdew, K. Burke, and M. Ernzerhof, Phys. Rev. Lett. **77**, 3865 (1996).
[44]G. Kresse and D. Joubert, Phys. Rev. B **59**, 1758 (1999).
[45]H. J. Monkhorst and J. D. Pack, Phys. Rev. B **13**, 5188 (1976).
[46]R. Hill, Proc. Phys. Soc., London A **65**, 349 (1952).
[47]D. Roundy, C. R. Krenn, M. L. Cohen, and J. W. Morris, Jr. Phys. Rev. Lett. **82**, 2713 (1999).
[48]R. F. Zhang, S. H. Sheng, and S. Veprek, Appl. Phys. Lett. **91**, 031906 (2007).
[49]J. O. Kim, J. D. Achenbach, P. B. Mirkarimi, M. Shinn, and S. A. Barnett, J. Appl. Phys. **72**, 1805 (1992).
[50]J. J. Gilman and B. W. Roberts, J. Appl. Phys. **32**, 1405 (1961).
[51]M. Born, Proc. Cambridge Philos. Soc. **36**, 160 (1940).
[52]F. Birch, Phys. Rev. **71**, 809 (1947).
[53]S. F. Pugh, Philos. Mag. **45**, 823 (1954).
[54]M. G. Zhang, H. Y. Yan, Q. Wei, and H. Wang, J. Appl. Phys. **112**, 013522 (2012).
[55]Y. Zhang, H. Sun, and C. F. Chen, Phys. Rev. Lett. **94**, 145505 (2005).
[56]R. F. Zhang, Z. J. Lin, Y. S. Zhao, and S. Veprek, Phys. Rev. B **83**, 092101 (2011).
[57]R. F. Zhang, Z. J. Lin, H. K. Mao, and Y. S. Zhao, Phys. Rev. B **83**, 060101(R) (2011).
[58]R. F. Zhang, D. Legut, Z. J. Lin, Y. S. Zhao, H. K. Mao, and S. Veprek, Phys. Rev. Lett. **108**, 255502 (2012).
[59]M. G. Zhang, H. Y. Yan, Y. R. Zhao, and Q. Wei, Comput. Mater. Sci. **83**, 457 (2014).
[60]R. F. Zhang, S. Veprek, and A. S. Argon, Phys. Rev. B **77**, 172103 (2008).
[61]R. F. Zhang, S. H. Sheng, and S. Veprek, Scr. Mater. **68**, 913 (2013).
[62]X. Q. Chen, H. Y. Niu, D. Z. Li, and Y. Y. Li, Intermetallics **19**, 1275 (2011).
[63]B. Bhushan and B. Gupta, *Handbook of Tribology Materials, Coatings, and Surface Treatments* (McCraw Hill, New York, 1991).